Stabilization of Excess Charge in Isolated Adenosine 5′-Triphosphate and Adenosine 5′-Diphosphate Multiply and Singly Charged Anions

Ruth M. Burke, Julie K. Pearce, William E. Boxford, Angelika Bruckmann, and Caroline E. H. Dessent*

Department of Chemistry, University of York, Heslington, York YO10 5DD, U.K.

Received: June 2, 2005; In Final Form: August 23, 2005

Multiply charged anions (MCAs) represent highly energetic species in the gas phase but can be stabilized through formation of molecular clusters with solvent molecules or counterions. We explore the *intramolecular* stabilization of excess negative charge in gas-phase MCAs by probing the intrinsic stability of the [adenosine 5′-triphosphate-2H]$^{2-}$ ([ATP-2H]$^{2-}$), [adenosine 5′-diphosphate-2H]$^{2-}$ ([ADP-2H]$^{2-}$), and $H_3P_3O_{10}^{2-}$ dianions and their protonated monoanionic analogues. The relative activation barriers for decay of the dianions via electron detachment or ionic fragmentation are investigated using resonance excitation of ions isolated within a quadrupole trap. All of the dianions decayed via ionic fragmentation demonstrating that the repulsive Coulomb barriers (RCB) for ionic fragmentation lie below the RCBs for electron detachment. Both the electrospray ionization mass spectra (ESI-MS) and total fragmentation energies for [ATP-2H]$^{2-}$, [ADP-2H]$^{2-}$, and $H_3P_3O_{10}^{2-}$ indicate that the multiply charged $H_3P_3O_{10}^{2-}$ phosphate moiety is stabilized by the presence of the adenosine group and the stability of the dianions increases in the order $H_3P_3O_{10}^{2-}$ < [ADP-2H]$^{2-}$ < [ATP-2H]$^{2-}$. Fully optimized, B3LYP/6-31+G* minimum energy structures illustrate that the excess charges in all of the phosphate anions are stabilized by intramolecular hydrogen bonding either within the phosphate chain or between the phosphate and the adenosine. We develop a model to illustrate that the relative magnitudes of the RCBs and hence the stability of these ions is dominated by the extent of intramolecular hydrogen bonding.

1. Introduction

The study of isolated, gas-phase multiply charged anions (MCAs) has developed into a rapidly expanding research field over recent years, with considerable experimental and theoretical effort being expended to provide preliminary insights into the electronic and geometric properties of MCAs.[1−13] Much of this research effort is driven by the challenge of understanding the unique physical characteristics of these systems. For example, the ground-state potential energy surfaces of MCAs are generally dominated by novel repulsive Coulomb barriers (RCBs) that arise from the combination of the long-range Coulomb repulsion between the excess negative charges and the short-range attractive interaction. These RCBs can impart electronic or thermodynamic metastability to an MCA, and a detailed understanding of the nature and effects of RCBs on the physical properties of MCAs is a focus of much current research.[2−6,9−12]

MCAs are common species in condensed phase environments since the local electric field provided by solvent molecules or counterions stabilizes the MCA with respect to Coulombic explosion. In contrast, the stabilizing local field is absent for an isolated gas-phase MCA and the Coulomb repulsion between the excess charges can therefore only be reduced via electron loss or ionic fragmentation. There have now been a number of gas-phase studies exploring the stabilization of MCAs by microsolvation (e.g. $SO_4^{2-}\cdot nH_2O$, $n = 1-40$, and dicarboxylate$^{2-}\cdot nH_2O$, $n = 1-10$)[7,13−17] and counterion complexation (e.g. $Na^+\cdot SO_4^{2-}$ and $Cs^+\cdot C_9^{2-}$).[18−20] However, little attention has been paid to *intramolecular* stabilization of multiple charges via noncovalent interaction with a covalently attached dielectric group.

In this paper, we address the issue of intramolecular stabilization of excess charge by investigating the intrinsic stability of gas-phase [adenosine 5′-triphosphate-*n*H]$^{n-}$ ([ATP-*n*H]$^{n-}$) and [adenosine 5′-diphosphate-*n*H]$^{n-}$ ([ADP-*n*H]$^{n-}$), $n = 1$ and 2, compared to the $H_3P_3O_{10}^{2-}$ and $H_4P_3O_{10}^{-}$ triphosphates. Figure 1 illustrates the chemical structures of the fully protonated forms of the ions. (The phosphate/ADP/ATP system is used here since it provides an ideal *chemical* system for exploring how the stability of an MCA evolves across a series of closely related molecular ions.) In general, a gas-phase MCA such as [ATP-2H]$^{2-}$ can be unstable with respect to decay via either electron detachment (eq 1a) or ionic fragmentation (eq 1b); i.e.

$$[\text{ATP-2H}]^{2-} \rightarrow [\text{ATP-2H}]^{-} + e^{-} \quad (1a)$$

$$[\text{ATP-2H}]^{2} \rightarrow [\text{ADP-H}]^{-} + PO_3^{-} \quad (1b)$$

The relevant potential energy surfaces for (1a) and (1b) are illustrated in Figure 2. To date, the majority of fundamental chemical physics studies aimed at understanding the detailed potential energy surfaces of multiply charged anions (e.g. the work of Wang, Simons, Compton, and Cederbaum) have focused very strongly on electron detachment decay. In a recent study,[9] we investigated the collisional excitation of a series of transition metal complex metal dianions, MX_6^{2-}, where M = Ir, Os, Re, and Pt and X = Cl and Br, and demonstrated that the repulsive Coulomb barrier for ionic fragmentation (RCB_{if}) lies below the RCB for electron detachment (RCB_{ed}) for each of these ions. Furthermore, we developed a simple model to rationalize the relative heights of the RCBs for ionic fragmentation of the MX_6^{2-} dianions, thus providing a new insight into the factors controlling the potential energy surfaces for ionic fragmentation of MCAs.

* Corresponding author. Fax: 44-1904-432516. E-mail: ced5@york.ac.uk.

10.1021/jp052937y CCC: $30.25
Published on Web 10/07/2005

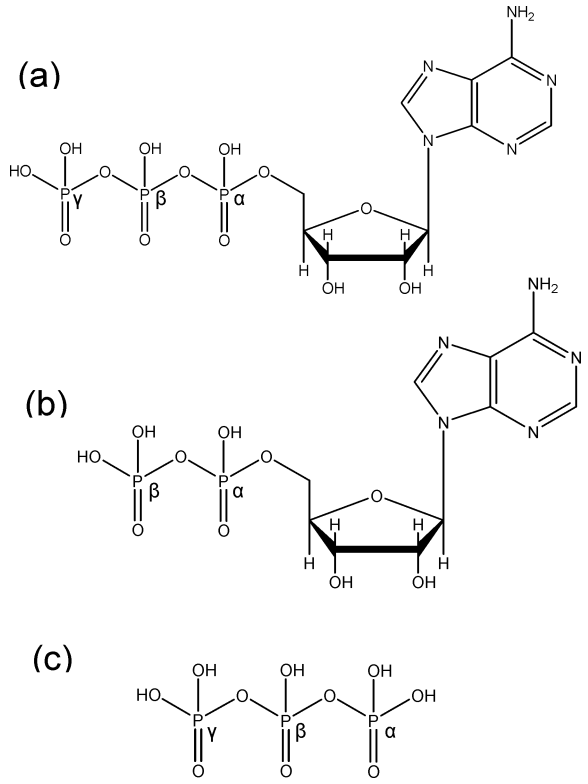

Figure 1. Chemical structures of the fully protonated forms of (a) ATP, (b) ADP, and (c) $H_5P_3O_{10}$. The α, *β*, and *γ* labels are used to define the tautomeric structures of the related anions.

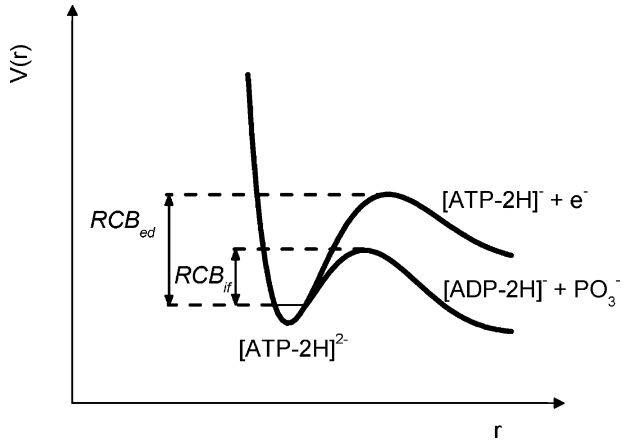

Figure 2. Potential energy surfaces (schematic) for dissociation of the $[ATP\text{-}2H]^{2-}$ dianion via ionic fragmentation and electron detachment. The RCBs(inner) for electron detachment (RCB_{ed}) and ionic fragmentation (RCB_{if}) are illustrated.

Our aim here is to extend our earlier work to investigate whether a similar model can be used to understand the relative RCBs for ionic fragmentation in a series of structurally related, covalently bonded MCAs. We employ a combination of electrospray ionization and quadrupole ion-trap mass spectrometry to establish whether the $[ATP\text{-}2H]^{2-}$, $[ADP\text{-}2H]^{2-}$, and $H_3P_3O_{10}^{2-}$ MCAs are indeed prone to decay via ionic fragmentation and to explore the relative stability of these MCAs. While laser spectroscopic measurements are desirable for detailed explorations of the MCA potential energy surfaces, quadrupole ion-trap mass spectroscopy can provide a straightforward and economical means to establish the relative activation energies for suitable groups of ions[21] and is, therefore, an ideal precursor to future laser spectroscopy studies.

ATP is a ubiquitous biological molecule that is found in all groups of organisms. It plays an essential biochemical role as the primary molecule through which energy is transmitted in living cells.[22] ATP carries multiple negative charges in the physiological pH range, and the Coulombic repulsion that exists between these excess charges contributes to the energy rich character of its phosphate bonds.[23] Although the study of biologically relevant molecules in the gas phase has represented a rapidly growing area of research in the past few years,[24−34] it is surprising that relatively little work has been conducted on the ATP system.[35,36] The ATP and ADP anions are of interest as model gas-phase biological molecules since their excess charges are expected to lead to cyclization due to intramolecular hydrogen-bond formation. This situation mirrors the much more widely recognized and studied cyclization of protonated peptides.[37] We present ab initio results to support previous hydration free energy measurements which indicated the presence of intramolecular hydrogen bonds in gas-phase $[ADP\text{-}2H]^{2-}$ dianions.[36]

2. Experimental Section

A Finnigan LCQ electrospray quadrupole ion trap mass spectrometer was employed for all experiments, run in negative ion mode. The signal was generally optimized using the automatic tuning capabilities of the LCQ, although additional spectra were recorded by manually varying the cone voltage (CV) from −2.2 to −4.2 kV and the capillary temperature (CT) from 70 to 250 °C to optimize the anion signals. Sample solution concentrations were $\sim 1 \times 10^{-3}$ M (80:20 methanol/water), prior to electrospraying in pure methanol at a flow rate of 3 μL/min. Compounds were purchased from Aldrich and used without further purification.

The mass spectra were obtained over a mass window of *m*/*z* 50−600 (lower *m*/*z* features are very poorly detected by the LCQ). Collision-induced dissociation (CID) (or *resonance excitation*) was performed on isolated ions by applying an excitation voltage to the trap end caps to induce collisions of the isolated anions with the helium buffer gas ($\sim 1 \times 10^{-4}$ Torr).[21] The application of a resonance excitation signal to the ion trap endcap electrodes matched to the secular frequency of the isolated ions induces an increase in the amplitude of axial motion of the ions and, therefore, an increase in the kinetic energy of the ions.[21,38] In contrast to CID experiments in triple quadrupole instruments,[39] the kinetic energy imparted to the ions is not well defined and is not the same for all masses. This fact, coupled with uncertainties as to the internal energies of the isolated ions, makes quantitative measurements of activation barrier extremely difficult. However, Brodbelt[40] has demonstrated that the threshold to dissociation using resonance excitation in a quadrupole ion trap is directly proportional to the decomposition activation barrier for ions of up to ∼100 amu in difference. We are therefore confident that we will be able to extract information concerning the relative decomposition activation barriers between ions of interest. The LCQ uses a Mathieu parameter (q_z) of 0.25 for resonance excitation, and ions are subject to a 30 ms excitation time. The excitation voltage amplitude was varied between 0 and 2.5 V zero-to-peak resonant excitation potential. CID energies are quoted as a percentage of 2.5 V in line with standard nomenclature.[41,42] Precursor ion excitation within the ion trap involves multiple low energy collisions with helium at a frequency of $\sim 10^4$ s^{-1} [21] and is therefore similar to thermal excitation in a hot, low-pressure gas. When the high-energy tail of the ion energy envelope reaches the activation energy for the lowest energy

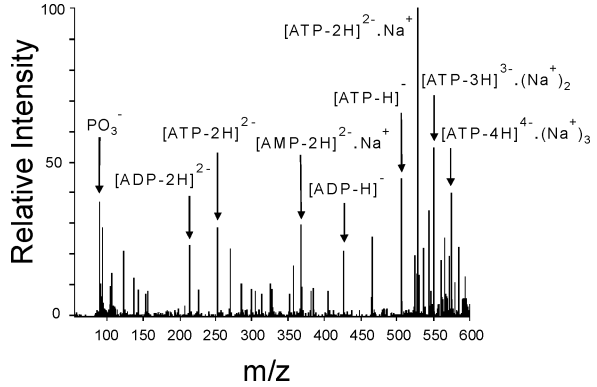

Figure 3. Negative ion ESI-MS of the sodium salt of ATP (tuning on $m/z = 252.5$), sprayed at a capillary temperature of 200 °C and a cone voltage of −2.2 kV.

decomposition pathway (i.e. the lower energy RCB), decomposition begins to occur and fragment ions are observed. Typical experimental errors for the fragment ion decay curves (obtained from repeat runs) were ±3%.

3. Computational Methods

Initial conformational searches for the 100 lowest energy conformers of each of the anions studied in this work were carried out using the Merk Molecular Force Field (MMFF94) as implemented in SPARTAN.[43] Conformational searches were conducted on a varying number of tautomers for each of the systems studied, as detailed in the results section. Single point energies were calculated for each of the resulting conformers at the B3LYP/6-31+G* level, and the lowest energy conformer obtained for each tautomer was then fully optimized (using default convergence criteria) in GAUSSIAN 03.[44] To test the reliability of this approach, four conformers were chosen at random from three sets of the tautomers and subjected to geometry optimization. The tests revealed that the relative energies of conformers remain unchanged upon full optimization, except where the single point energies varied by less than 0.1 eV. In such cases, optimization of all structures with similar relative energies was therefore essential. (This situation only occurred for the α,*β*-tautomer of ATP^{2-}.)

Frequencies were calculated for all optimized species to confirm the geometries were minima on the potential energy surface.

4. Experimental Results

4.1. $[ATP\text{-}nH]^{n-}$ ($n = 1, 2$). Figure 3 displays the negative ion ESI-MS of the sodium salt of ATP (CT of 200 °C). The singly charged species, $[ATP\text{-}2H]^{2-}\cdot Na^+$, $[ATP\text{-}3H]^{3-}\cdot 2Na^+$, $[ATP\text{-}H]^-$, and $[ATP\text{-}4H]^{4-}\cdot 3Na^+$, are the main species observed, with the doubly charged $[ATP\text{-}2H]^{2-}$ ion appearing at $m/z = 252.5$ with slightly lower intensity than the singly charged ions. The presence of the $[ADP-H]^-$ peak indicates that ionic fragmentation of ATP can occur either in the bulk solution or within the mass spectrometer's source region. Decreasing the CT further increased the relative abundance of impurity peaks (i.e. ion−solvent clusters), while increasing the CT reduced the impurity peaks but also reduced the intensity of $[ATP\text{-}2H]^{2-}$. Neither $[ATP\text{-}3H]^{3-}$ nor $[ATP\text{-}4H]^{4-}$ was present in the ESI-MS, despite the fact that these ions are known to exist in bulk solution at the experimental pH. The absence of these ions could be attributed to a number of causes including their intrinsic instability with respect to ionic fragmentation, rapid protonation within solvent microdroplets during the final stages of the ESI desolvation, or preferential formation of ion-pair complexes such as $[ATP\text{-}3H]^{3-}\cdot 2Na^+$ within the ESI microdroplets. A list of the main peaks present under the various ESI-MS conditions employed is displayed in Table 1S, available in the Supporting Information.

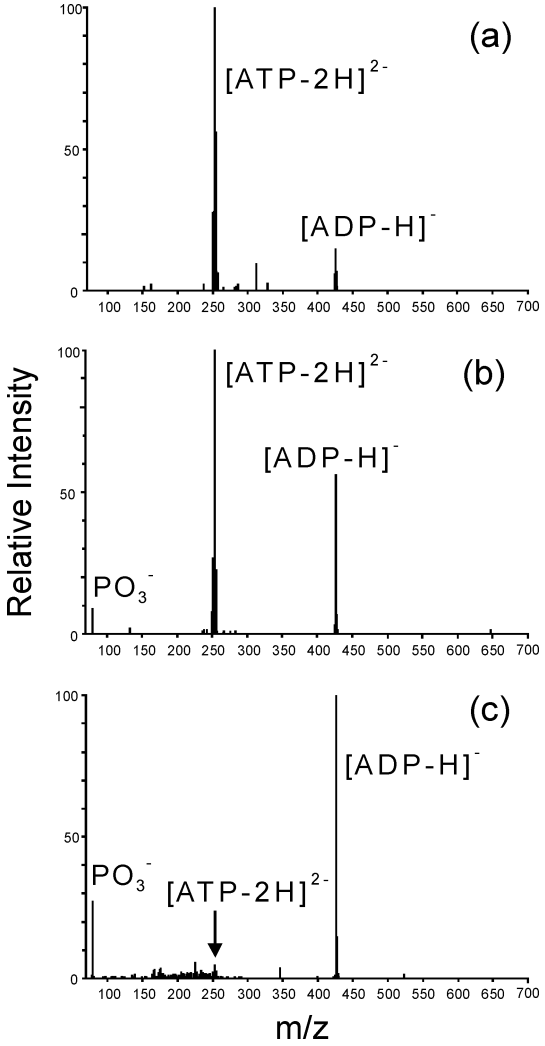

Figure 4. (a) Isolation of $[ATP\text{-}2H]^{2-}$ in the quadrupole trap at 0% collision energy, (b) CID mass spectrum of $[ATP\text{-}2H]^{2-}$ at 5% collision energy, and (c) that at 25% collision energy, illustrating fragmentation into $[ADP-H]^-$ and PO_3^-.

The doubly charged $[ATP\text{-}2H]^{2-}$ dianion was isolated in the quadrupole ion trap (Figure 4a) and subjected to resonance excitation to investigate its decay pathways. Even at 0% collision energy (Figure 4a), $[ATP\text{-}2H]^{2-}$ can be seen to decay with production of $[ADP-H]^-$. A similar effect has been observed in previous CID studies of multiply charged ions[9,41] and can be attributed to the dissociation of metastable parent dianions that are thermally or collisionally activated as they travel through the mass spectrometer. Figure 4b,c displays the resulting fragment ion mass spectra obtained at 5% and 25% collision energy, illustrating that $[ATP\text{-}2H]^{2-}$ decays into $[ADP-H]^-$ and PO_3^- upon resonance excitation. (The lower m/z PO_3^- ion is not detected as efficiently as the higher mass fragments in the LCQ, and therefore, the product ions do not appear with identical intensities.) Figure 5 displays the $[ATP\text{-}2H]^{2-}$ CID fragmentation results as a function of collision energy, illustrating that the dianion is almost entirely fragmented at 25% collision energy.

The fragment ions observed upon resonance excitation of $[ATP\text{-}2H]^{2-}$ are consistent with ionic fragmentation of the

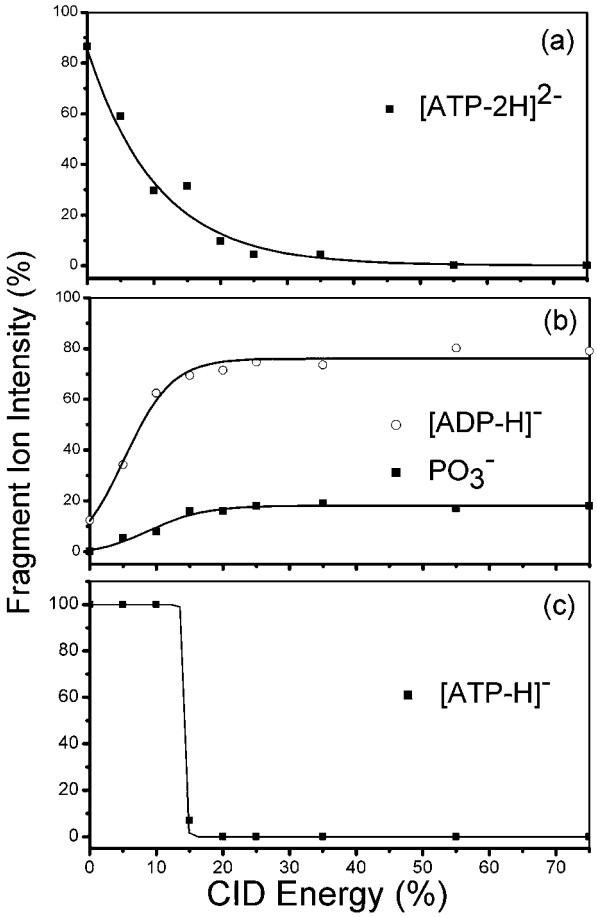

Figure 5. % fragmentation curves for (a) decay of the $[ATP\text{-}2H]^{2-}$ parent dianion into (b) the $[ADP\text{-}H]^-$ and PO_3^- product fragment ions and (c) decay of the $[ATP\text{-}H]^-$ parent anion. Typical experimental errors (obtained from repeat runs) were ±3%.

"high-energy" phosphate bond (eq 1b). $[ATP\text{-}2H]^-$ is not produced upon excitation of the dianion, a notable result given the widespread view that gas-phase dianions are primarily unstable with respect to electron detachment. These observations indicate that RCB_{if}(inner) lies below RCB_{ed}(inner) for $[ATP\text{-}2H]^{2-}$, as illustrated schematically in Figure 2.

To investigate the effect of charge state on the fragmentation pathway of the molecular ion, the $[ATP-H]^-$ monoanion was isolated in the quadrupole ion trap and subjected to resonance excitation. Figure 5c displays the $[ATP\text{-}H]^-$ fragmentation results as a function of collision energy. The dominant fragmentation channel at lower collision energies corresponds to loss of H_3PO_4 with production of the associated $C_{10}H_{12}N_5P_2O_9^-$ anionic fragment. At higher collision energies, a number of additional minor fragmentation channels appear. The % fragmentation curves for the product ion changes are included as Supporting Information (Figure 1S).

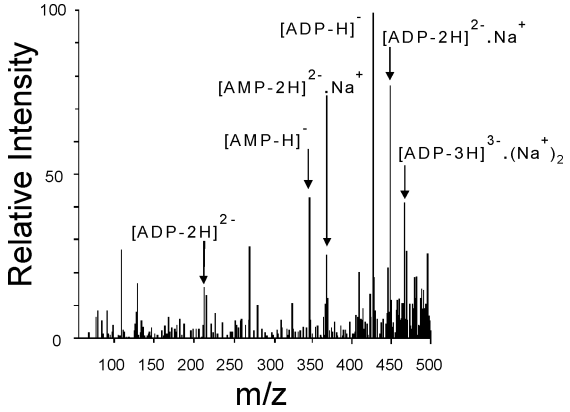

Figure 6. Negative ion ESI-MS of the sodium salt of ADP (tuning on $m/z = 212.5$), sprayed at a capillary temperature of 200 °C and a cone voltage of −4.2 kV.

Our main purpose in using the fragment onset curves displayed in Figure 5 is that it provides a fuller picture of the fragmentation characteristics than single CID-MS. CID fragment ion intensities are influenced by the mass and degrees of freedom of the parent ion and by kinetic shifts, but in general the maximum collision energy converted to internal energy is proportional to the relative collision energy and inversely proportional to the parent ion mass.[21,41] (In using this approach to compare ions of similar m/z values but with different charges, we are following the previous work of ref 41.) Since $[ATP\text{-}2H]^{2-}$ and $[ATP\text{-}H]^-$ differ by only a single mass unit, the CID curves provide a good indication of the relative barrier heights for fragmentation. In evaluating the fragmentation energetics of different ions, it is useful to compare the collision energy required to deplete the parent ion concentration by half (E_{half}). For $[ATP\text{-}2H]^{2-}$ E_{half} requires 8% collision energy, whereas $[ATP\text{-}H]^-$ requires 15% collision (Table 1), reflecting the intrinsic instability of the multiply charged ion compared to the monoanion due to the presence of uncompensated coulomb repulsion. Finally, we note the distinctive, sharp fragmentation onset of the $[ATP\text{-}H]^-$ monoanion compared to the $[ATP\text{-}2H]^{2-}$ dianion studied above; this appears to reflect differences in the potential energy surfaces of the singly and multiply charged anions across the dissociation thresholds.

4.2 ADP^{n-} ($n = 1, 2$). Figure 6 displays the negative ion ESI-MS of the sodium salt of ADP (CT of 200 °C). The spectrum has an appearance similar to that of the ATP ESI-MS presented above (Figure 3), with the main species corresponding to the singly charged moieties, $[ADP\text{-}H]^-$, $[ADP\text{-}3H]^{3-}\cdot 2Na^+$, and $[ADP\text{-}2H]^{2-}\cdot Na^+$, while the doubly charged $[ADP\text{-}2H]^{2-}$ ion is present at lower intensity at $m/z = 212.5$. The presence of the $[AMP\text{-}H]^-$ ion again indicates that ADP fragmentation has occurred in the bulk solution or within the mass spectrometer's source region. At higher CT (275 °C), the spectrum is again much cleaner, although the $[ADP\text{-}2H]^{2-}$ dianion is now

TABLE 1: ESI-MS and CID Results for the $[ATP\text{-}nH]^{n-}$ and $[ADP\text{-}nH]^{n-}$ ($n = 1$ and 2), $H_3P_3O_{10}^{2-}$, and $H_4P_3O_{10}^-$ Anions

parent ion	m/z_{obs}	BPI_{max}[a] (%)	fragment: 0% CID	fragment(s): 5% CID	E_{half}[b]	E_{full}[c]
$[ATP\text{-}2H]^{2-}$	252.5	29	$[ADP\text{-}H]^-$	$[ADP\text{-}H]^-$, PO_3^-	8	46
$[ADP\text{-}2H]^{2-}$	212.5	15	$[AMP\text{-}H]^-$	$[AMP\text{-}H]^-$, PO_3^-	6	31
$H_3P_3O_{10}^{2-}$	128	10	$H_3P_2O_7^-$	$H_3P_2O_7^-$, PO_3^-	–	14
$[ATP\text{-}H]^-$	506	95	–	–	15	17
$[ADP\text{-}H]^-$	426	100	–	–	14	16
$H_4P_3O_{10}^-$	257	36	–	–	–	20

[a] Maximum achievable base peak intensity of parent ion in ESI-MS. [b] Collision energy necessary to deplete the parent ion intensity by half. [c] Collision energy necessary to induce total fragmentation of parent ion.

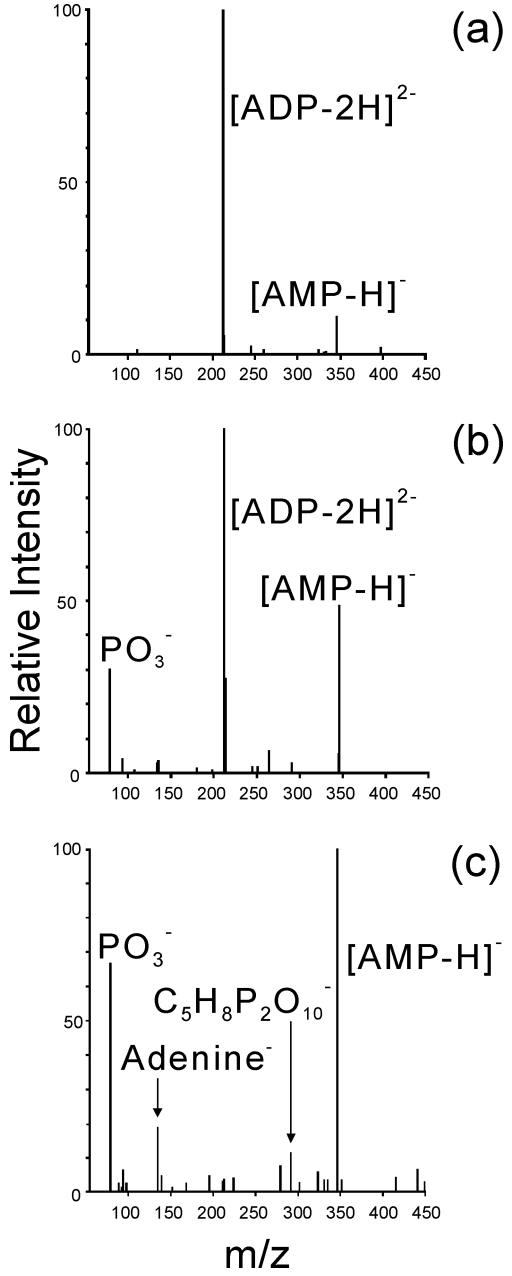

Figure 7. (a) Isolation of $[ADP\text{-}2H]^{2-}$ in the quadrupole trap at 0% collision energy, (b) CID mass spectrum of $[ADP\text{-}2H]^{2-}$ at 5% collision energy, and (c) that at 25% collision energy, illustrating fragmentation of $[ADP\text{-}2H]^{2-}$ into $[AMP\text{-}H]^{-}$ and PO_3^{-}. At 25% collision energy, a new fragmentation channel is evident corresponding to fragmentation of $[ADP\text{-}2H]^{2-}$ into adenine^{-} and $C_5H_8P_2O_{10}^{-}$.

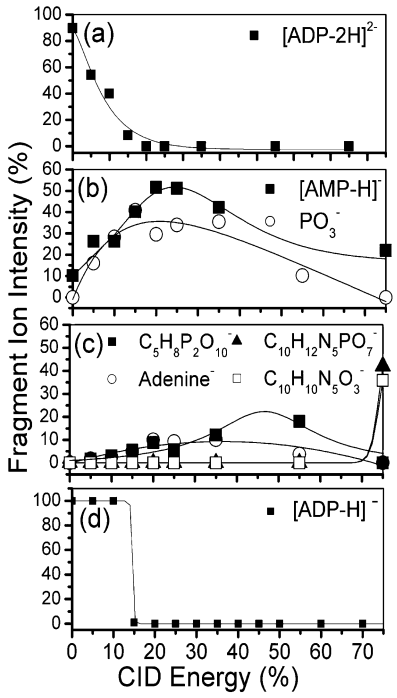

Figure 8. % fragmentation curves for (a) decay of the $[ADP\text{-}2H]^{2-}$ parent dianion into (b) the $[AMP-H]^{-}$ and PO_3^{-} product fragment ions, (c) minor product fragment ions, and (d) % fragmentation curve for decay of the $[ADP\text{-}H]^{-}$ anion.

entirely absent, indicating its lower intrinsic stability compared to the larger $[ATP\text{-}2H]^{2-}$ analogue.

$[ADP\text{-}2H]^{2-}$ was isolated in the quadrupole ion trap (Figure 7a) and subjected to resonance excitation to investigate its decay pathways. Figure 7b,c displays the resulting CID spectra obtained at 5% and 25% collision energy. $[ADP\text{-}2H]^{2-}$ behaves like $[ATP\text{-}2H]^{2-}$ at 0% and 5% collision energy, as it fragments across the phosphate bond with production of the $[AMP\text{-}H]^{-}$ and PO_3^{-} anions. At 25% collision energy, a new fragmentation channel is evident with rupture of the adenine−ribose bond occurring to produce adenine(−) and $C_5H_8P_2O_{10}^{-}$, i.e. $[ADP\text{-}2H-\text{adenine}]^{-}$ anions. Figure 8 displays the $[ADP\text{-}2H]^{2-}$ CID fragmentation results as a function of collision energy and illustrates that the dianion is almost entirely fragmented at 20% collision energy. Above 30% collision energy, the $[AMP\text{-}H]^{-}$ fragment intensity decreases sharply and new fragment ions appear ($C_{10}H_{10}N_5O_3^{-}$, i.e. adenosine−H_2O, and $C_{10}H_{11}N_5PO_6^{-}$, i.e. [cyclic AMP-H]$^{-}$). E_{half} for the parent $[ADP\text{-}2H]^{2-}$ dianion is 6% collision energy, compared to 8% collision energy for $[ATP\text{-}2H]^{2-}$. This reflects the lower intrinsic stability of the smaller $[ADP\text{-}2H]^{2-}$ dianion.

To investigate the effect of charge state on the fragmentation pathway of the molecular ion, the $[ADP\text{-}H]^{-}$ monoanion was isolated in the quadrupole ion trap and subjected to resonance excitation. Figure 8d displays the $[ADP\text{-}H]^{-}$ fragmentation results as a function of collision energy. As for the $[ATP\text{-}H]^{-}$ anion, the dominant fragmentation channel at lower collision energies corresponds to loss of H_3PO_4, with a number of additional minor fragmentation channels appearing at higher collision energies. The % fragmentation curves for the product ion channels are included as Supporting Information (Figure 2S). E_{half} for the $[ADP\text{-}2H]^{2-}$ dianion is 6% collision energy, compared to 14% collision energy for $[ADP\text{-}H]^{-}$. As in the ATP system, this result reflects the intrinsic instability of the multiply charged $[ADP\text{-}2H]^{2-}$ compared to the $[ADP\text{-}H]^{-}$ monoanion.

4.3. $H_3P_3O_{10}^{2-}$ and $H_4P_3O_{10}^{-}$ Anions. The $P_3O_{10}^{5-}$ moiety represents the phosphate chain, i.e. the primary charge carrier in ATP, and the fragmentation of $H_3P_3O_{10}^{2-}$ and $H_4P_3O_{10}^{-}$ was therefore investigated as a comparison to the $[ATP\text{-}nH]^{n-}$, $n =$ 1 and 2, ions. The required phosphate species proved challenging to detect under all the ESI-MS conditions employed, with the $H_3P_3O_{10}^{2-}$ dianion appearing weakly at low CT (i.e. 70 °C). At high CT (275 °C), the intensities of the $H_3P_2O_7^{-}$ and PO_3^{-} ions increased, indicating that the $H_3P_3O_{10}^{2-}$ dianion is prone to ionic fragmentation within the ESI source. No $H_3P_3O_{10}^{-}$ is evident in the ESI-MS, indicating that $H_3P_3O_{10}^{2-}$ does not spontaneously decay via electron detachment. We emphasize that the greater abundance of $[ATP\text{-}2H]^{2-}$ in the ESI-MS presented in section 4.1 compared to the $H_3P_3O_{10}^{2-}$ dianion (cf. Table S2) suggests that the adenosine group provides effective stabilization of the excess negative charges. This point will be

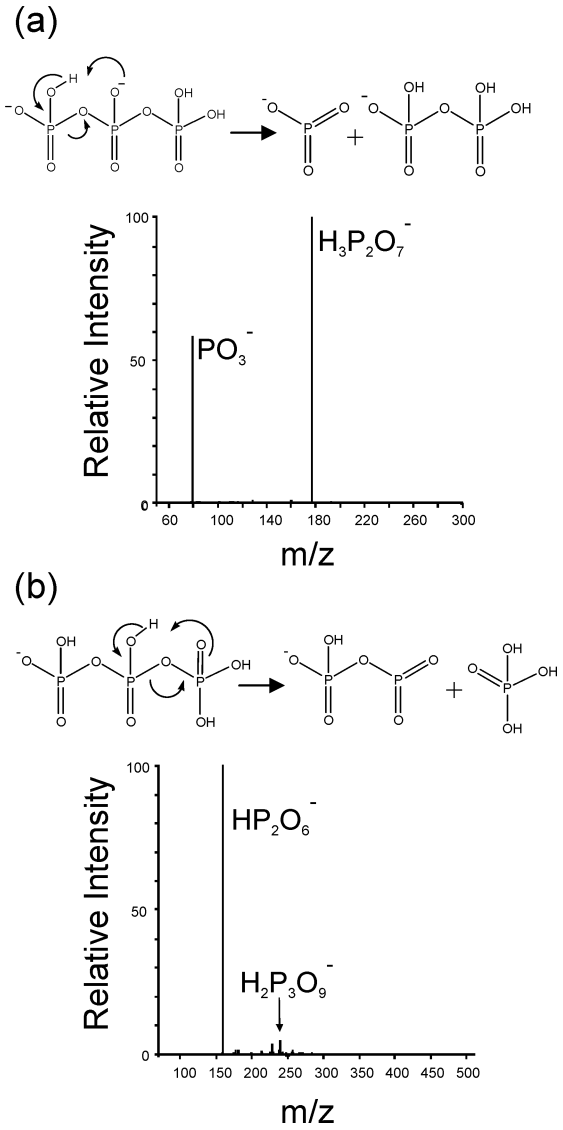

Figure 9. CID mass spectra of (a) $H_3P_3O_{10}^{2-}$ illustrating complete fragmentation of the parent dianion into the $H_3P_2O_7^-$ and PO_3^- product fragments at 14% collision energy and (b) $H_4P_3O_{10}^-$ illustrating complete fragmentation of the parent anion into $HP_2O_6^-$ via loss of H_3PO_4 at 20% collision energy. Possible fragmentation mechanisms are illustrated.

discussed further in section 6. A list of the main peaks present under the various ESI-MS conditions employed is displayed in Table 2S, available in the Supporting Information.

To investigate whether RCB_{if} or RCB_{ed} is the lowest energy decay pathway, the $H_3P_3O_{10}^{2-}$ parent dianion was isolated in the quadrupole ion trap and activated using resonance excitation. As expected from the ESI-MS, the $H_3P_3O_{10}^{2-}$ dianion decays with production of $H_3P_2O_7^-$ and PO_3^- upon resonance excitation (Figure 9a). A possible fragmentation mechanism is illustrated. The production of $H_3P_2O_7^-$ and PO_3^- unambiguously demonstrates that $H_3P_3O_{10}^{2-}$ decays via ionic fragmentation (analogous to pathway (1b)). We therefore conclude that RCB_{if}(inner) again lies below RCB_{ed}(inner) for the $H_3P_3O_{10}^{2-}$ dianion. The CID spectrum presented in Figure 9a was recorded at 14% collision energy, the resonance excitation energy at which the parent dianion had completely decayed into products. Due to the difficulty in electrospraying $H_3P_3O_{10}^{2-}$ in our mass spectrometer, it was not possible to obtain % fragmentation curves for this dianion. However, the relatively low collision energy for total breakdown of $H_3P_3O_{10}^{2-}$ (14%) compared to $[ATP\text{-}2H]^{2-}$ (46%) and $[ADP\text{-}2H]^{2-}$ (31%) is consistent with $H_3P_3O_{10}^{2-}$ being intrinsically less stable than the ATP/ADP analogues.

The CID fragment mass spectrum of the $H_4P_3O_{10}^-$ monoanion obtained at a collision energy of 20% is displayed in Figure 9b for comparison with the corresponding $H_3P_3O_{10}^{2-}$ dianion. By analogy with the $[ATP\text{-}H]^-$ and $[ADP\text{-}H]^-$ monanions studied above, $H_4P_3O_{10}^-$ fragments predominantly with loss of H_3PO_4 producing the $HP_2O_6^-$ ion. Figure 9b illustrates a possible fragmentation mechanism. A second, very minor fragmentation channel is also evident on the CID-MS consistent with loss of H_2O from the parent anion.

It is notable that resonance excitation of $H_3P_3O_{10}^{2-}$ and $H_4P_3O_{10}^-$ leads to decay with the production of the same product fragments as the respective larger ions; i.e., $H_3P_3O_{10}^{2-}$ decays in the same way as $[ATP\text{-}2H]^{2-}$, etc. The fragmentation energetics therefore appear to be dominated by the phosphate chain, and the ATP and ADP anions should display fragmentation mechanisms similar to the ones illustrated for $H_3P_3O_{10}^{2-}$ and $H_4P_3O_{10}^-$ in Figure 9.

5. Computational Results

5.1. $H_3P_3O_{10}^{2-}$ and $H_4P_3O_{10}^-$. Figure 1c illustrates the labeling scheme used to describe the tautomers of $H_3P_3O_{10}^{2-}$; for example, $\alpha\alpha$ refers to the tautomer where both excess charges are centered on the α phosphate group. Only tautomers $\alpha\beta$ and $\alpha\gamma$ of $H_3P_3O_{10}^{2-}$ were subjected to conformational searches in SPARTAN, since tautomer $\alpha\alpha$ should lie higher in energy due to the substantial Coulombic repulsion that would exist between adjacent negative charges.

Figure 10 displays the optimized structures and relative energies of tautomers $\alpha\beta$ and $\alpha\gamma$, obtained following the procedure described in section 3. Key geometric parameters are displayed in Table 2. Each of the optimized structures displays three intramolecular hydrogen bonds, which we classify as either typical (<3 Å, 180 ± 25°) or loose (<3.5 Å, 180 ± 65°).[45] For conformers I−V, the three hydrogen bonds are all involved in stabilizing the excess charges, whereas conformer VI lies at higher energy as only two of the hydrogen bonds involve the negative charges. Conformers I−V all adopt cyclic structures, with the conformers only differing in the positions of the hydrogen bonds while the positions of the atoms are similar. This means that the distances between the oxygen atoms are comparable, so that the Coulombic repulsion in the $\alpha\beta$ and $\alpha\gamma$ tautomers is similar. In fact, the lowest energy conformer is an $\alpha\beta$-tautomer, presumably due to the fact that the primary hydrogen bond (4,5) is able to adopt a more optimum geometry than in the $\alpha\gamma$-tautomer conformer II. We note that the identification of an $\alpha\beta$-tautomer as the lowest energy tautomer is consistent with the proposed fragmentation mechanism displayed in Figure 9a. The results obtained are in good agreement with previous B3LYP/TZVP+(modified) results.[47]

Figure 11 illustrates the optimized conformers and energies of $H_4P_3O_{10}^-$ obtained at the B3LYP/6-31+G* level of theory, with key geometric parameters again listed in Table 2. As in $H_3P_3O_{10}^{2-}$, the preferred conformation corresponds to a cyclical head-to-tail arrangement (conformers I−IV). We note that the two lowest energy conformers differ only in the position of a single hydrogen atom and could readily interconvert at ambient temperatures, hence facilitating fragmentation in line with the mechanism displayed in Figure 9b. The highest energy noncyclic conformer, V, closely resembles the highest energy conformer, VI, of $H_3P_3O_{10}^{2-}$ (Figure 10). The preference for cyclic structures and the geometry of the global minimum again agree well with the previous B3LYP/TZVP+ results.[47]

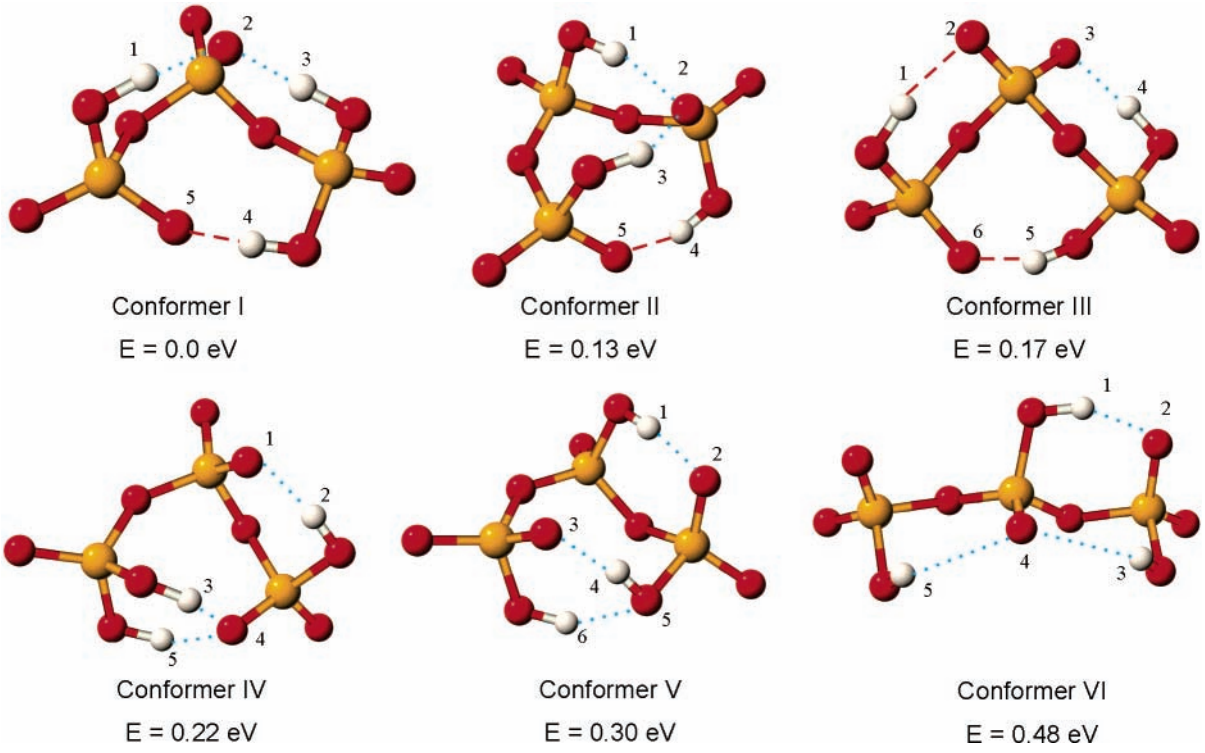

Figure 10. Minimum energy structures of $H_3P_3O_{10}^{2-}$ calculated at the B3LYP/6-31+G* level. The atom-labeling scheme and relative energies are illustrated. Typical hydrogen bonds are indicated as red dashed lines, with loose "hydrogen-bond-like" interactions as blue dotted lines.[45]

TABLE 2: Key Geometric Parameters for the Minimum Energy Structures of $H_3P_3O_{10}^{2-}$ and $H_4P_3O_{10}^{-}$ Calculated at the B3LYP/6-31+G* Level[a]

	conformer																	
	I			II			III			IV			V			VI		
$H_3P_3O_{10}^{2-}$																		
bond	1,2	2,3	4,5	1,2	2,3	4,5	1,2	3,4	5,6	1,2	3,4	4,5	1,2	3,4	5,6	1,2	3,4	4,5
angle (deg)	146	151	170	144	152	163	156	153	157	149	147	150	149	145	150	146	116	123
length (Å)	1.732	1.536	1.392	1.665	1.520	1.446	1.753	1.623	1.492	1.616	1.569	1.519	1.536	1.500	1.790	1.627	2.383	2.299
$H_4P_3O_{10}^{-}$																		
bond	1,2	3,4	5,6	1,2	3,4	5,6	1,2	2,3	4,5	1,2	3,4	3,5	1,2	2,3	4,5	5,6		
angle (deg)	147	152	132	147	133	151	139	151	164	148	147	143	149	149	149	149		
length (Å)	1.634	1.631	2.030	1.673	2.166	1.497	1.723	1.552	1.625	1.671	1.581	1.695	1.748	1.746	1.746	1.746		

[a] Atom labels follow Figures 10 and 11, with bond angles of $O-H^x\text{--}O^y$ labeled by the *x* and *y* atom labels.

5.2. [ATP-*n*H]$^{n-}$ (*n* = 1, 2). For the ATP and ADP systems, we present only the lowest energy conformer of the lowest energy tautomer for simplicity. The orthophosphate results presented above illustrate some of the types of conformational flexibility and relative conformer energies that also occur for the [ATP-*n*H]$^{n-}$ and [ADP-*n*H]$^{n-}$, *n* = 1 and 2, ions. While a variety of conformational structures will clearly be populated under the experimental conditions employed, the lowest energy structures are generally representative of a range of the populated lower energy conformers, which display only modest structural differences. The lowest energy conformers presented are more than adequate for providing a basis for a discussion of the structural factors that influence the relative stability of the ions (section 6).

The lowest energy tautomer of $[ATP\text{-}2H]^{2-}$ was found to correspond to a structure where the negative charges reside on the phosphate groups nearest the adenosine, i.e. the $\alpha\beta$-tautomer. Figure 12a displays the lowest energy conformer of the $\alpha\beta$-tautomer obtained at the B3LYP/6-31+G* level, with key geometric parameters being displayed in Table 3. In the lowest energy structure, the phosphate chain adopts a cyclic structure where the excess charges are stabilized by intramolecular hydrogen bonds, in a structural motif that resembles the lowest energy conformer of $H_3P_3O_{10}^{2-}$ (Figure 10). The primary hydrogen bonds connect the H1 of the γ-phosphate to the O2 of the α-phosphate and the O8 of the β-phosphate to the H7 of the ribose sugar. Three additional weak, hydrogen-bonding type interactions are also present, connecting H9 of the γ-phosphate to the O8 of the β-phosphate, the two OH groups of the ribose (i.e. H5 and O6), and the O3 of the phosphate chain to the H4 of adenine.

For the singly charged $[ATP\text{-}H]^{-}$, the lowest energy tautomer (Figure 12b) corresponds to a structure where the negative charge resides on the α-phosphate (O2 and O8) adjacent to the adenosine. This situation contrasts with the related $H_4P_3O_{10}^{-}$ anion where the lowest energy tautomer accommodates the negative charge on the β-phosphate (Figure 11). In the lowest energy $[ATP\text{-}H]^{-}$ conformer, the primary hydrogen bonds exist between the H1 of the γ-phosphate and the O2 of the α-phosphate group and the O8 of the α-phosphate and the H7 of the ribose. These dominant interactions mirror those of the lowest energy conformer of $[ATP\text{-}2H]^{2-}$ (Figure 12a). In addition, weaker hydrogen-bonding-like interactions exist between the H9 of the β-phosphate and the O8 of the α-phosphate,

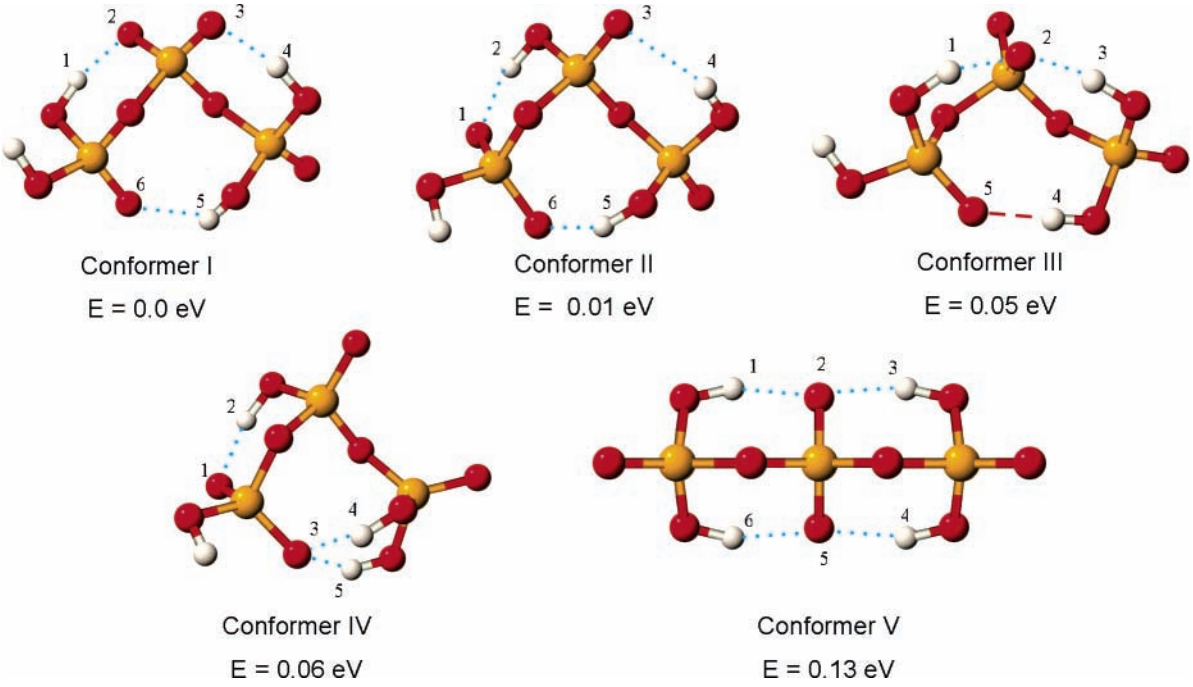

Figure 11. Minimum energy structures of $H_4P_3O_{10}^-$ calculated at the B3LYP/6-31+G* level. The atom-labeling scheme and relative energies are illustrated. Typical hydrogen bonds are indicated as red dashed lines, with loose "hydrogen-bond-like" interactions as blue dotted lines.[45]

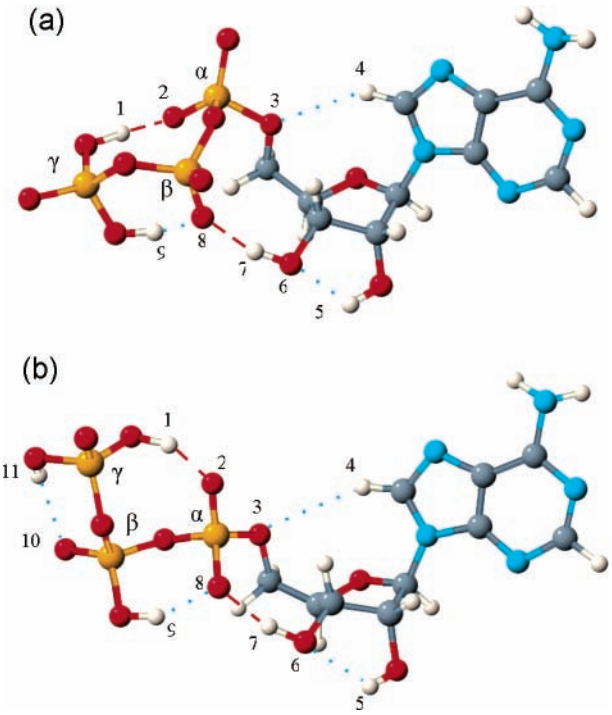

Figure 12. Global minimum energy structures of (a) $[ATP\text{-}2H]^{2-}$ and (b) $[ATP\text{-}H]^-$ calculated at the B3LYP/6-31+G* level. The atom-labeling scheme and relative energies are illustrated. Typical hydrogen bonds are indicated as red dashed lines, with loose "hydrogen-bond-like" interactions as blue dotted lines.[45]

the H11 of the γ-phosphate and the O10 of the β-phosphate, the two OH groups (i.e. H5 and O6) of the ribose, and the O3 of the phosphate chain to the H4 of adenine. The previous two interactions again resemble ones found in the lowest energy $[ATP\text{-}2H]^{2-}$ conformer. Key geometric parameters are displayed in Table 3.

5.3. $[ADP\text{-}nH]^{n-}$ ($n = 1, 2$). The lowest energy tautomer of $[ADP\text{-}2H]^{2-}$ corresponds to a structure where one negative charge resides on each of the two phosphate groups, i.e. an $\alpha\beta$-tautomer. Figure 13a displays the lowest energy conformer of the $\alpha\beta$-tautomer obtained at the B3LYP/6-31+G* level, with key geometric parameters presented in Table 3. For this ion, the primary hydrogen bonds exist between the O4 of the β-phosphate and the H3 and H5 atoms of the sugar; a unique structural motif that is not observed in the minimum energy structures of $[ADP\text{-}H]^-$ or the $[ATP\text{-}nH]^{n-}$, $n = 1$ and 2, ions. An additional, loose hydrogen bond is also present between the H2 of the β-phosphate and the O1 of the α-phosphate, an interaction that is present in all of the $[ATP\text{-}nH]^{n-}$ and $[ADP\text{-}nH]^{n-}$ conformers shown in Figures 12 and 13.

For the singly charged $[ADP\text{-}H]^-$ anion, the lowest energy tautomer corresponds to an α-tautomer where the negative charge resides on the phosphate adjacent to the adenosine. Figure 13b displays the lowest energy conformer obtained at the B3LYP/6-31+G* level, with key geometric parameters being included in Table 3. The primary hydrogen bonding interaction in this structure occurs between the O2 of the α-phosphate and

TABLE 3: Key Geometric Parameters for the Minimum Energy Structures of the $[ATP\text{-}nH]^{n-}$ and $[ADP\text{-}nH]^{n-}$ ($n = 1, 2$) Ions Calculated at the B3LYP/6-31+G* Level[a]

			$[ATP\text{-}2H]^{2-}$			
bond	1,2	3,4	5,6	7,8	8,9	
angle (deg)	170	151	122	167	152	
length (Å)	1.396	3.036	1.914	1.563	1.529	
			$[ATP\text{-}H]^-$			
bond	1,2	3,4	5,6	7,8	8,9	10,11
angle (deg)	168	151	118	156	145	148
length (Å)	1.496	3.036	2.039	1.623	1.735	2.216
			$[ADP\text{-}2H]^{2-}$			
bond	1,2	3,4	4,5			
angle (deg)	151	159	171			
length (Å)	1.630	1.535	1.703			
			$[ADP\text{-}H]^-$			
bond	1,2	2,3	4,5	6,7		
angle (deg)	153	162	120	152		
length (Å)	1.870	1.694	1.963	1.879		

[a] Atom labels follow Figures 12 and 13, with bond angles of $O-H^x\text{--}O^y$ labeled by the x and y atom labels.

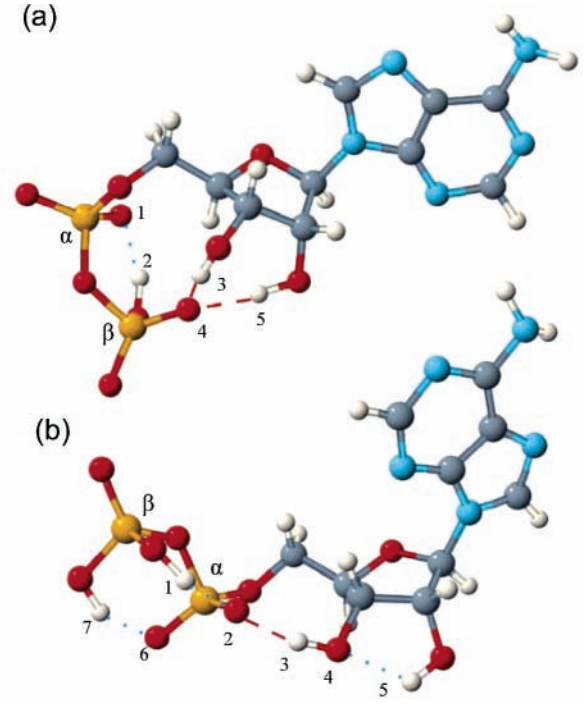

Figure 13. Global minimum energy structures of (a) $[ADP\text{-}2H]^{2-}$ and (b) $[ADP\text{-}H]^{-}$ calculated at the B3LYP/6-31+G* level. The atom-labeling scheme and relative energies are illustrated. Typical hydrogen bonds are indicated as red dashed lines, with loose "hydrogen-bond-like" interactions as blue dotted lines.[45]

the H3 of the ribose. Additional, loose hydrogen-bonding type interactions exist between the H1 and H7 groups on the β-phosphate to the O2 and O6 oxygens of the α-phosphate group (an arrangement similar to that for the $[ATP\text{-}2H]^{2-}$ structure displayed in Figure 12a) and between the adjacent OH groups of the ribose (i.e. H5 and O4).

5.4. Comparison of the DFT and MMFF94 Results. While it is beyond the scope of this manuscript to provide an in depth analysis of the differences between the fully optimized structures of the $[ATP\text{-}n\mathrm{H}]/[ADP\text{-}n\mathrm{H}]^{n-}$, $n = 1$ and 2, anions presented above and the MMFF94 molecular mechanics results, several points are of note. In general, a geometric structure that is obtained from the MMFF94 procedure will not change significantly when subjected to full optimization at the B3LYP/6-31+G* level. The overall molecular conformation remains the same, with the same number and type of hydrogen-bonding interactions. However, this does not imply that the molecular mechanics results are equivalent to the DFT results since the energetic ordering of the conformers obtained from the molecular mechanics method changes when the B3LYP/6-31+G* energies are calculated. This has significant consequences for the experiments conducted here and would be even more important if the calculations were being used to support spectroscopic measurements. For example, using MMFF94, the lowest energy $[ATP\text{-}2H]^{2-}$ conformer displays two typical and two loose intramolecular hydrogen bonds but the lowest energy $[ADP\text{-}2H]^{2-}$ conformer also displays two typical and two loose intramolecular hydrogen bonds. Therefore, the molecular mechanics results would provide no explanation for the difference in stability of the $[ATP\text{-}2H]^{2-}$ and $[ADP\text{-}2H]^{2-}$ multiply charged anions. This contrasts with the B3LYP results, which indicate that the lowest energy $[ATP\text{-}2H]^{2-}$ conformer displays two additional loose hydrogen bonds compared to $[ADP\text{-}2H]^{2-}$. The B3LYP results therefore support the experiment observation that $[ADP\text{-}2H]^{2-}$ is intrinsically less stable than $[ATP\text{-}2H]^{2-}$.

6. Further Discussion

Upon isolation and resonance excitation in a quadrupole trap, the $[ATP\text{-}2H]^{2-}$, $[ADP\text{-}2H]^{2-}$, and $H_3P_3O_{10}^{2-}$ dianions all decay via ionic fragmentation of the orthophosphate bond to produce PO_3^- and the respective residual anion. No electron detachment products were observed, even at relatively high collision energies. This observation reflects the fact that RCB_{ed}(inner) is substantially higher than RCB_{if}(inner) for these dianions, mirroring results obtained in our group for transition metal complex dianions.[9] Although gas-phase molecular dianions are commonly thought to be primarily unstable with respect to electron detachment, our results illustrate that ionic fragmentation will generally represent the preferred lowest energy decay pathway for dianions that can dissociate to form stable anions. While larger multiply charged biomolecular ions such as peptides and oligonucleotides have also been observed to dissociate via ionic fragmentation, these situations are somewhat different from the systems studied here where the excess charges occupy adjacent molecular groups.[48−50]

Comparing the ESI-MS and % collision energies necessary to achieve total fragmentation (E_{full}) of $[ATP\text{-}2H]^{2-}$, $[ADP\text{-}2H]^{2-}$, and $H_3P_3O_{10}^{2-}$ illustrates the *intramolecular* stabilization of multiple charges via noncovalent interaction with a covalently attached group. We noted in section 4.2 that the resonance excitation experiments reveal that $[ATP\text{-}2H]^{2-}$ is intrinsically more stable than $[ADP\text{-}2H]^{2-}$, i.e. RCB_{if}(inner)$[ATP\text{-}2H]^{2-}$ > RCB_{if}(inner)$[ADP\text{-}2H]^{2-}$. This result is intriguing since although the charge-carrying phosphate chain is smaller in ADP than ATP, our calculations indicate that the excess charges will be accommodated on adjacent phosphate groups in both dianions, producing very similar quantities of intramolecular Coulombic repulsion.

In a recent paper, we proposed a model to illustrate the physical origin of the RCB_{if} for a MX_6^{2-} dianion, where M = Ir, Re, and Rh and X = Cl and Br.[8] The inner RCB_{if} was found to be associated with the purely attractive binding energy of the monoanions; i.e.

$$RCB_{if}(\text{inner}) = \Delta E(MX_5^- + X^-) - \text{intramolecular Coulomb repulsion} \quad (2)$$

With extension of this model to the dianions studied here,

$$RCB_{if}(\text{inner}) = \Delta E(PO_3^- + \text{monanion}) + \Delta E(\text{intramolecular noncovalent interactions}) - \text{intramolecular Coulomb repulsion} \quad (3)$$

where, $\Delta E(PO_3^- + \text{monoanion})$ is the covalent bond energy of the orthophosphate bond, which will be very similar for $[ATP\text{-}2H]^{2-}$, $[ADP\text{-}2H]^{2-}$, and $H_3P_3O_{10}^{2-}$, and the second term gives the energy associated with noncovalent interactions in the dianion.

The origin of the relative stability of $[ATP\text{-}2H]^{2-}$ compared to $[ADP\text{-}2H]^{2-}$ can therefore be traced to differences in the intramolecular noncovalent interactions present in the minimum energy conformers. In a comparison of the structures displayed in Figures 12a and 13a, the intramolecular interactions within $[ATP\text{-}2H]^{2-}$ and $[ADP\text{-}2H]^{2-}$ will be dominated by hydrogen bonds, and while $[ATP\text{-}2H]^{2-}$ possesses two typical and three loose hydrogen bonds, $[ADP\text{-}2H]^{2-}$ possesses only two typical and one loose hydrogen bonds. The presence of two additional hydrogen-bonding type interactions in $[ATP\text{-}2H]^{2-}$ increases the magnitude of RCB_{if}(inner), making this dianion intrinsically more stable than $[ADP\text{-}2H]^{2-}$. Similarly, the minimum energy

$H_3P_3O_{10}^{2-}$ structure (Figure 10) possesses a single typical hydrogen bond, along with two loose hydrogen bonds, consistent with its reduced stability compared to both $[ATP\text{-}2H]^{2-}$ and $[ADP\text{-}2H]^{2-}$.

The relative stabilities of the phosphate dianions can therefore be rationalized with reference to the extent and strength of intramolecular hydrogen bonding within the ions. This mirrors the known stabilization of multiply charged anions with respect to both ionic fragmentation and electron detachment via sequential solvation with water molecules.[6,14−17,51,52] Nonetheless, the intrinsic stability of the dianions studied will also be affected by the extent of dielectric screening that exists between the excess charges. This effect is implicitly included within the third term of eq 3, where any dielectric screening acts to reduce the overall intramolecular Coulomb repulsion.

Williams and co-workers have conducted a number of detailed studies exploring the extent of dielectric stabilization of charge in, for example, diprotonated diaminoalkanes and multiply protonated gramicidin S.[49,50] For the diprotonated diaminoalkanes, an average ϵ_r value of 1.01 ± 0.07 was obtained indicating that the gas-phase shielding provided by the molecular $(CH_2)_n$ groups of the two distinct positive charges was negligible.[52] The intrinsic dielectric polarizability of gramicidin S was a similar value of <1.2.[53] These low ϵ_r values were attributed to the dominant influence of the surrounding vacuum medium (permittivity = 1.00). By analogy, we would anticipate a similar low value of ϵ_r for the adenosine group, so that the overall effect on the RCB_{if}(inner) heights in $[ATP\text{-}2H]^{2-}$and $[ADP\text{-}2H]^{2-}$ should be small. Nonetheless, the absence of the adenosine group in the $H_3P_3O_{10}^{2-}$ dianion reduces the dielectric available for charge stabilization (hence increasing the magnitude of the intramolecular Coulomb repulsion term in (3)) and, therefore, contributes to the relative instability of $H_3P_3O_{10}^{2-}$.

The results presented in this work provide a preliminary insight into the effect of intramolecular stabilization of excess negative charges in gas-phase multiply charged anions. Laser photodetachment−photoelectron spectroscopy would be highly useful to quantify the effects observed here, since photodetachment measurements of $[ATP\text{-}2H]^{2-}$, $[ADP\text{-}2H]^{2-}$, and $H_3P_3O_{10}^{2-}$ would give a spectroscopic measurement of the dianions' intramolecular Coulomb repulsion [i.e. $RCB_{ed}(outer) = RCB_{if}(outer)$][2,9] and, hence, quantify the effect of dielectric stabilization of the excess charges. Complementary laser scans across the region of RCB_{if}(inner)[12] would similarly quantify the extent of the intramolecular stabilization of excess charge through noncovalent interactions.

The B3LYP/6-31+G* minimum energy structures of $[ATP\text{-}nH]^{n-}$, $[ADP\text{-}nH]^{n-}$, $H_3P_3O_{10}^{2-}$, and $H_4P_3O_{10}^{-}$ presented in section 5 illustrate that the excess charges in all of the phosphate systems are stabilized by intramolecular hydrogen bonding either within the phosphate chain or between the phosphate and the adenosine. It is useful to consider the gas-phase hydration free energies of $[ADP\text{-}2H]^{2-}$ in the context of our calculations. Kebarle and co-workers found that the hydration energies for $[ADP\text{-}2H]^{2-}$ were much weaker than for the related $H_2P_2O_7^{2-}$ diphosphate dianion.[36] On the basis of space-filling models, the authors interpreted this result as evidence for the presence of intramolecular hydrogen bonds within the ADP dianion, suggesting that a hydrogen bond formed between the anionic oxygen on the terminal phosphate and the 3′ hydroxyl group of the ribose (O4 to H3 in Figure 13a). This interaction is indeed present in our $[ADP\text{-}2H]^{2-}$ minimum energy conformer displayed in Figure 13a, resulting in a structure where the excess charge available to an external solvent molecule is reduced compared to $H_2P_2O_7^{2-}$.

While the stabilization of excess charge via cyclization due to intramolecular hydrogen bonding is a well-known effect in protonated and polyprotonated peptides,[37] it is much less established for negatively charged systems.[36,47] This is despite the likely importance of such interactions in many important biomolecular anions such as nucleic acids,[50,54] where the presence of intramolecular hydrogen bonds is likely to affect the collision induced dissociation results of bioanalytic sequencing experiments.[55] The B3LYP/6-31+G* calculations presented in section 5 should therefore provide a useful reference point for discussing the conformational and tautomeric structures of related bioanions and, hence, interpreting their mass spectrometric data.

Acknowledgment. C.E.H.D. thanks the Royal Society for support from a Royal Society University Research Fellowship. We thank the EPSRC for support from Grant EP/C51212X/1 and for the award of computer time (CHEM/294) at the Rutherford Appleton Laboratories under the auspices of the Computational Chemistry Working Party. We also thank Dr. Trevor Dransfield for essential mass spectrometry support.

Supporting Information Available: Tables of ESI-MS results for the sodium salts of ATP and $H_5P_3O_{10}$ as a function of cone temperature and cone voltage. This material is available free of charge via the Internet at http://pubs.acs.org.

References and Notes

(1) Schauer, S. N.; Williams, P.; Compton, R. N. *Phys. Rev. Lett.* **1990**, *65*, 625.
(2) Wang, X. B.; Yang, X.; Wang, L. S. *Int. Rev. Phys. Chem.* **2002**, *21*, 473.
(3) Schröder, D. *Angew. Chem., Int. Ed.* **2004**, *43*, 1329.
(4) Dreuw, A.; Cederbaum, L. S. *Chem. Rev.* **2002**, *102*, 181.
(5) Scheller, M. K.; Compton, R. N.; Cederbaum, L. S. *Science* **1995**, *270*, 116.
(6) Boldyrev, A. I.; Gutowski, M.; Simons, J. *Acc. Chem. Res.* **1996**, *29*, 497.
(7) Blades, A. T.; Kebarle, P. *J. Am. Chem. Soc.* **1994**, *116*, 10761.
(8) Compton, R. N.; Tuinman, A. A.; Klots, C. E.; Pederson, M. R.; Patton, D. C. *Phys. Rev. Lett.* **1997**, *78*, 4367.
(9) Boxford, W. E.; Pearce, J. K.; Dessent, C. E. H. *Chem. Phys. Lett.* **2004**, *399*, 465.
(10) Ehrler, O. T.; Furche, F.; Weber, J. M.; Kappes, M. M. *J. Chem. Phys.* **2005**, *122*, 94321.
(11) Boltalina, O. V.; Streletskii, A. V.; Ioffe, I. N.; Hvelplund, P.; Liu, B.; Nielsen, S. B.; Tomita, S. *J. Chem. Phys.* **2005**, *122*, 21102.
(12) Friedrich, J.; Gilb, S.; Ehrler, O. T.; Behrendt, A.; Kappes, M. M. *J. Chem. Phys.* **2002**, *117*, 2635.
(13) Wong, R. L.; Williams, E. R. *J. Phys. Chem. A* **2003**, *107*, 10976.
(14) Wang, X. B.; Nicholas, J. B.; Wang, L. S. *J. Chem. Phys.* **2000**, *113*, 10837.
(15) Ding, C. F.; Wang, X. B.; Wang, L. S. *J. Phys. Chem. A* **1998**, *102*, 8633.
(16) Dessent, C. E. H.; Rigby, C. *Chem. Phys. Lett.* **2003**, *370*, 52.
(17) Kambalapalli, S.; Ortiz, J. V. *J. Phys. Chem. A* **2003**, *107*, 10360.
(18) Wang, X. B.; Ding, C. F.; Nicholas, J. B.; Dixon, D. A.; L. S. Wang, *J. Phys. Chem. A* **1999**, *103*, 3423.
(19) Vandenbosch, R.; Will, D. I.; Cooper, C.; Henry, B.; Liang, J. F. *Chem. Phys. Lett.* **1997**, *274*, 112.
(20) Dreuw, A.; Cederbaum, L. S. *J. Chem. Phys.* **1999**, *111*, 1467.
(21) March, R. E.; Todd, J. F. *Practical Aspects of Ion-Trap Mass Spectrometry*; CRC Press: Boca Raton, FL, 1995; Vols. 1 and 2.
(22) Westheimer, F. H. *Science* **1987**, *235*, 1173.
(23) Rees, D. C.; Howard, J. B. *J. Mol. Biol.* **1999**, *293*, 343.
(24) Simons, J. P. *Phys. Chem. Chem. Phys.* **2004**, *6*, E7.
(25) Wyttenbach, T.; Bowers, M. T. *Top. Curr. Chem.* **2003**, *225*, 207.
(26) McLafferty, F. W.; Fridriksson, E. K.; Horn, D. M. *Science* **1999**, *284*, 1289.
(27) Jarrold, M. F. *Acc. Chem. Res.* **1999**, *32*, 360.
(28) Xu, S. J.; Zheng, W. J.; Radisic, D.; Bowen, K. H. *J. Chem. Phys.* **2005**, *122*, 091103.

(29) Srebalus Barnes, C. A.; Clemmer, D. E. *J. Phys. Chem. A* **2003**, *107*, 10566.
(30) Wang, X.; Levy, D. H.; Rubin, M. B. *J. Phys. Chem. A* **2000**, *104*, 6558.
(31) Porath, D.; Bezryadin, A.; de Vries, S.; Dekker, C. *Nature* **2000**, *403*, 635.
(32) Ullrich, S.; Tarczay, G.; Tong, X.; Dessent, C. E. H.; Müller-Dethlefs, K. *Phys. Chem. Chem. Phys.* **2001**, *3*, 5450.
(33) Fricke, H.; Gerlach, A.; Unterberg, C.; Rzepecki, P.; Schrader, T.; Gerhards, M. *Phys. Chem. Chem. Phys*. **2004**, *6*, 4636.
(34) Desfrancois, C.; Abdoul-Carime, H.; Schermann, J. P. *J. Chem. Phys.* **1996**, *104*, 7792.
(35) Julian, R. R.; Beauchamp J. L. *Int. J. Mass Spectrom.* **2003**, *227*, 147.
(36) Blades, A. T.; Ho, Y.; Kebarle, P. *J. Phys. Chem.* **1996**, *100*, 2443.
(37) Davies, J. S. *J. Pept. Sci.* **2003**, *9*, 471.
(38) Splendore, M.; Londry, F. A.; March, R. E.; Morrison, R. J. S.; Perrier, P.; André, J. *Int. J. Mass Spectrom. Ion Processes* **1996**, *156*, 11.
(39) Armentrout, P. B. *J. Am. Soc. Mass Spectrom.* **2002**, *13*, 419.
(40) Colorado, A.; Brodbelt, J. S. *J. Am. Soc. Mass Spectrom.* **1996**, *7*, 1116.
(41) a) Ince, M. P.; Perera, B. A.; Van Stipdonk, M. J. *Int. J. Mass. Spectrom.* **2001**, *207*, 41. (b) Vachet, R. W.; Callahan, J. H, *J. Mass Spectrom.* **2000**, *35*, 311.
(42) Satterfield, M.; Brodbelt, J. S. *Inorg. Chem.* **2001**, *40*, 5393.
(43) Deppmeier, B. J.; Driessen, A. J.; Hehre, T. S.; Hehre, W. J.; Johnson, J. A.; Klunzinger, P. E.; Leonard, J. M.; Ohlinger, W. S.; Pham, I. N.; Pietro, W. J.; Yu, J. *PC Spartan Pro*; Wavefunction, Inc.: Irvine, CA, 2000.
(44) Frisch, M. J.; Trucks, G. W.; Schlegel, H. B.; Scuseria, G. E.; Robb, M. A.; Cheeseman, J. R.; Montgomery, J. A., Jr.; Vreven, T.; Kudin, K. N.; Burant, J. C.; Millam, J. M.; Iyengar, S. S.; Tomasi, J.; Barone, V.; Mennucci, B.; Cossi, M.; Scalmani, G.; Rega, N.; Petersson, G. A.; Nakatsuji, H.; Hada, M.; Ehara, M.; Toyota, K.; Fukuda, R.; Hasegawa, J.; Ishida, M.; Nakajima, T.; Honda, Y.; Kitao, O.; Nakai, H.; Klene, M.; Li, X.; Knox, J. E.; Hratchian, H. P.; Cross, J. B.; Adamo, C.; Jaramillo, J.; Gomperts, R.; Stratmann, R. E.; Yazyev, O.; Austin, A. J.; Cammi, R.; Pomelli, C.; Ochterski, J. W.; Ayala, P. Y.; Morokuma, K.; Voth, G. A.; Salvador, P.; Dannenberg, J. J.; Zakrzewski, V. G.; Dapprich, S.; Daniels, A. D.; Strain, M. C.; Farkas, O.; Malick, D. K.; Rabuck, A. D.; Raghavachari, K.; Foresman, J. B.; Ortiz, J. V.; Cui, Q.; Baboul, A. G.; Clifford, S.; Cioslowski, J.; Stefanov, B. B.; Liu, G.; Liashenko, A.; Piskorz, P.; Komaromi, I.; Martin, R. L.; Fox, D. J.; Keith, T.; Al-Laham, M. A.; Peng, C. Y.; Nanayakkara, A.; Challacombe, M.; Gill, P. M. W.; Johnson, B.; Chen, W.; Wong, M. W.; Gonzalez, C.; Pople, J. A. *Gaussian 03*, revision C.01; Gaussian, Inc.: Pittsburgh, PA, 2003.
(45) The term "hydrogen bond" is applied to any pairwise interaction between an electron-pair-donating atom and an electron-pair-accepting hydrogen atom.[46] We define typical hydrogen bonds as having bond lengths <3 Å and angles of $180 \pm 25°$, with loose "hydrogen-bond-like" interactions having bond lengths <3.5 Å and angles of $180 \pm 65°$. It should be noted that a hydrogen bond typically has a length of ~ 2 Å and an angle of 180°.
(46) Liu, D.; Wyttenbach, T.; Carpenter, C. J.; Bowers, M. T. *J. Am. Chem. Soc.* **2004**, *126*, 3261.
(47) Wang, X. B.; Vorpagel, E. R.; Yang, X.; Wang, L. S. *J. Phys. Chem. A* **2001**, *105*, 10468.
(48) Loo, J. A.; Udesth, H. R.; Smith, R. D. *Rapid Commun. Mass Spectrom.* **1988**, *2*, 207.
(49) McLuckey, S. A.; Van Berkel, G. J.; Glish, G. L. *J. Am. Soc. Mass Spectrom.* **1992**, *3*, 60.
(50) McLuckey, S. A.; Habibi-Goudarzi, S. *J. Am. Chem. Soc.* **1993**, *115*, 12085.
(51) Boxford, W. E.; Dessent, C. E. H. *J. Phys. Chem. A* **2005**, *109*, 5836.
(52) Gross, D. S.; Rodriguez-Cruz, S. E.; Bock, S.; Williams, E. R. *J. Phys. Chem. A* **1995**, *99*, 4034.
(53) Gross, D. S.; Williams, E. R. *J. Am. Chem. Soc.* **1995**, *117*, 883.
(54) Rodgers, M. T.; Campbell, S.; Marzluff, E. M.; Beauchamp, J. L. *Int. J. Mass. Spectrom. Ion Processes* **1994**, *137*, 121.
(55) Bruni, R.; Gianfranceschi, G.; Koch, G. *J. Pept. Sci.* **2005**, *11*, 225.